NASA TECHNICAL NOTE

NASA TN D-5739

c. 1

NASA TN D-5739

WATER INJECTION FROM A 9° HEMISPHERE-CONE INTO A HYPERSONIC AIRSTREAM

by William L. Weaver and William F. Hinson

Langley Research Center
Langley Station, Hampton, Va.

NATIONAL AERONAUTICS AND SPACE ADMINISTRATION • WASHINGTON, D. C. • MARCH 1970

1. Report No. NASA TN D-5739	2. Government Accession No.	3. Recipient's Catalog No.
4. Title and Subtitle WATER INJECTION FROM A 9° HEMISPHERE-CONE INTO A HYPERSONIC AIRSTREAM		5. Report Date March 1970 6. Performing Organization Code
7. Author(s) William L. Weaver and William F. Hinson		8. Performing Organization Report No. L-6714 10. Work Unit No. 730-00-01-01-23
9. Performing Organization Name and Address NASA Langley Research Center Hampton, Va. 23365		11. Contract or Grant No. 13. Type of Report and Period Covered Technical Note
12. Sponsoring Agency Name and Address National Aeronautics and Space Administration Washington, D.C. 20546		14. Sponsoring Agency Code
15. Supplementary Notes		

16. Abstract

Wind-tunnel tests in which water was injected from the sides of a 0.375-scale model of the RAM C spacecraft through single- and multiple-orifice nozzles were made at nominal Mach numbers of 7.3 and 10.4. Photographs and plots of the water spray are presented. The measured outer limit of the water spray with single-orifice injection was in agreement with that predicted by a previous correlation equation. The maximum penetration with the multiple-orifice nozzle tests was correlated by the dynamic-pressure ratio at the injection site.

17. Key Words Suggested by Author(s) Water injection Hypersonic Mach number Penetration	18. Distribution Statement Unclassified – Unlimited		
19. Security Classif. (of this report) Unclassified	20. Security Classif. (of this page) Unclassified	21. No. of Pages 32	22. Price* $3.00

*For sale by the Clearinghouse for Federal Scientific and Technical Information
Springfield, Virginia 22151

WATER INJECTION FROM A 9° HEMISPHERE-CONE INTO A HYPERSONIC AIRSTREAM

By William L. Weaver and William F. Hinson
Langley Research Center

SUMMARY

Wind-tunnel tests in which water was injected from the sides of a 9° hemisphere-cone (0.375-scale model of the RAM C spacecraft) through single- and multiple-orifice nozzles were made at nominal Mach numbers of 7.3 and 10.4. Photographs and plots of the water spray are presented. The measured outer limit of the water spray with single-orifice injection was in agreement with that predicted by a previous correlation equation. The maximum penetration with the multiple-orifice nozzle tests was correlated by the dynamic-pressure ratio at the injection site.

INTRODUCTION

Project RAM (Radio Attenuation Measurements) at the Langley Research Center has for several years studied the problem of radio-frequency signal blackout produced by ionization surrounding a spacecraft during high-speed entry into the earth's atmosphere. The injection of liquid from the spacecraft into the ion plasma has been investigated in Project RAM as a technique for solving the entry communications problem. Three flight experiments have been conducted to test the technique. In two of these, water was injected from the sides and stagnation region of a 9° hemisphere-cone spacecraft at entry speeds of 5486 m/sec (ref. 1) and 7620 m/sec (ref. 2) (RAM B2 and C-I, respectively). In the third test (ref. 3), water was injected from the GT-3 spacecraft during entry. In these three tests, the effectiveness of relative amounts of water was compared by injection through several nozzles containing different numbers of orifices. The concentrations of the electrons in the flow field depend on the entry altitude and velocity and the size and shape of the spacecraft, and the effectiveness of a liquid to create a window through which signals may be transmitted by eliminating electrons depends on both the amount and the proper distribution of the liquid in the flow field.

Several test programs have been conducted since the initiation of Project RAM to study the penetration and distribution of liquid injectants in hypersonic airflow. In reference 4, water and liquid nitrogen were injected through single-orifice nozzles from the sides and stagnation region of several blunt models including a scale model of the

RAM B2 spacecraft. Considerable testing with injection from single-orifice nozzles from flat-plate models was done prior to these tests (refs. 5 to 11, for example), and the relationship between injection from a flat plate and that from a three-dimensional blunt body had not been established. In reference 3, water was injected through a single-orifice nozzle from a scale model of the GT-3 spacecraft and through a pattern of several orifices from the floor of the wind tunnel. No significant differences in penetration were observed between these two types of injection. In the analyses of the data from the RAM B2 flight and the injection experiment on the GT-3 flight, the penetration values used were based on the injection tests with single-orifice nozzles. The results of these analyses of the RAM B2 and the GT-3 flights are presented in references 1 and 3, respectively.

Prior to the flight of RAM C-I, a wind-tunnel test program was conducted in which water was injected through simulated nozzles of the flight injection system from the sides of a 0.375-scale model of the RAM C spacecraft. Also included were some tests with injection through single-orifice nozzles. The tests were made in the Ames 3.5-foot hypersonic wind tunnel at nominal Mach numbers of 7.3 and 10.4. Tunnel conditions and water pressure were varied to simulate a range of entry altitude conditions. The results of these tests are presented in this paper.

SYMBOLS

C_D	aerodynamic drag coefficient of jet
D_j	jet diameter (single orifice)
L_j	unit length of jet
m_j	water flow rate from all orifices (both sides of model)
m_B	airflow rate through stream tube area equal to base area of model
M	Mach number
p	pressure
p_w	water pressure at orifices
q	dynamic pressure

$\frac{\rho_j V_j^2}{\rho_\infty V_\infty^2}$ or $\frac{\rho_j V_j^2}{\rho_L V_L^2}$ dynamic-pressure ratio

T temperature

t time

V velocity

x,y coordinates defined in figure 6

x',y' coordinates defined in figure 6

$\Delta y'$ maximum penetration of water spray relative to model surface

ρ density

Subscripts:

j water jet before breakup

t total condition in tunnel reservoir

∞ free stream

L local airflow conditions at injection site

TEST FACILITY AND APPARATUS

Wind Tunnel

The tests were conducted in the Ames 3.5-foot hypersonic wind tunnel. This facility is of the blowdown type capable of operating at nominal Mach numbers of 5, 7, and 10 at total pressures up to 13.55×10^6 N/m^2. Total airstream temperatures up to 1170° K are available for test times up to 4 minutes. Helium is injected through an annular slot in the subsonic section of the nozzle to provide a layer of cool gas along the nozzle and test-section walls. A simplified diagram of the facility is presented in figure 1.

Test Model and Nozzles

The model used in the investigation was a 0.375-scale model of the RAM C spacecraft. Photographs of the model plan view and installation in the Ames 3.5-foot hypersonic wind tunnel are presented in figures 2 and 3, respectively. Figure 4 presents a schematic of the model and injection nozzles with pertinent details and dimensions. The model had a 5.715-cm-radius hemisphere followed by a 9^{o} half-angle conical frustum. Model shell structure was constructed from stainless steel which provided adequate heat sink capability to prevent damage to the model. The two wedge fins at the model base simulated the Langmuir probe configurations used on the full-scale spacecraft. The model was sting-mounted with a six-component strain-gage balance. The balance measured changes in aerodynamic forces and moments produced by the injected water; however, these measurements are not included in this paper. The model nose structure was constructed to receive interchangeable screw-in circular plugs which contained the various nozzles (designated nozzles A, B, C, D, and E) shown in figure 4. The single orifices of nozzles D and E are flush with the model surface. All plugs, when installed in the model, interfaced with the plenum chamber in the model nose structure.

Water Injection System

Figure 5 is a schematic of the water injection system. Pressure for the system was provided by a high-pressure gaseous nitrogen source. The nitrogen pressure was regulated according to the particular test condition. The distilled water was filtered with a 10-μm filter to insure particle-free water at the orifices. The flowmeter measured the water flow rates. Water "on and off" was controlled by a remotely operated piston valve located in the model nose adjacent to the nozzle plenum chamber. A pressure transducer was located in the plenum chamber to measure water pressure at the nozzle.

TEST CONDITIONS

The data presented and discussed herein were obtained after the tunnel had reached steady-state conditions. Total pressure and temperature in the tunnel supply reservoir were monitored and recorded during all tests. Water pressure in the model plenum chamber and the water flow rate were measured and were used to determine the exit velocity of the water jets. A thermocouple measured water temperature in the plenum chamber, and the temperature was found to remain approximately 289^{o} K during all tests.

Table I lists each nozzle tested and several pertinent conditions for each test. Also listed are several calculated flow parameters. The local aerodynamic flow properties (ρ_L and V_L) were computed at the injection site on the model in the absence of water flow. The technique employed included real-gas effects. Measurements of water spray were made on only one side of the model, since the penetration is the same on both sides because of flow symmetry.

RESULTS AND DISCUSSION

Basic Data

The measurements of the outer limit of the water spray were made from schlieren photographs. A sketch of the coordinate system and pertinent penetration terms used herein are presented in figure 6. For the configurations with nozzles A, B, D, and E, the origin of the coordinate system is the model station corresponding to the center line of the forward-most orifice; with nozzle C, the origin is the model station corresponding to the center line of the second set of orifices from the nose. The reason for this choice will become apparent in a subsequent discussion.

Figures 7 and 8 present photographs and plots of the measured outer limits of the water spray. Pertinent test conditions are shown. The plots of figure 8 show that for particular schlieren photographs the number of x,y points which could be measured varied because as the water spray was swept downstream the outer limit became less discernible and also the complete model could not be photographed because of limitations due to the size of the schlieren window.

Jet Shielding

The schlieren photographs in figure 7 with nozzle C show that beginning with the second row of jets in that nozzle there is an increased penetration over that of the first row. Photographic comparisons of injection for nozzles A and C at similar test conditions can be seen in the following figures: 7(a) with 7(b), 7(c) with 7(d), 7(k) with 7(*l*), and 7(m) with 7(n). Figures 8(a) and 8(b) show the comparison plots of these tests. The comparisons of figure 8(a) are at a Mach number of 7.26 and those of figure 8(b) are at a Mach number of 10.37. The photographic comparisons indicate that the initial penetration from the first set of jets in nozzle C is approximately the same as that from nozzle A at similar test conditions, and the comparison plots show a significant increase in the outer limit of the water when nozzle C is used.

The sketch of the hole pattern of nozzle C in figure 4 shows that the holes in the second row are alined longitudinally behind those of the first row. Apparently the jets from the first row of holes produce an area of low dynamic pressure in their wake and

thereby permit increased initial penetration of the jets from holes located in the low-pressure region. It cannot be determined from the photographs (fig. 7) if all the jets behind the first row are penetrating the same distance. The photographs of figures 7(g) to 7(j), which show two comparisons between injection from nozzles B and C at similar test conditions, indicate that the increased penetration seen with nozzle C is not present with nozzle B. The sketch of the hole pattern of nozzle B in figure 4 shows that no holes are alined directly behind others and thus no jets would be directly in the wake of other jets.

Mach Number Effect

Figures 7(e) and 7(f) compare photographs of injection from nozzle C at Mach numbers of 7.26 and 10.57. The water-system pressure was adjusted between the tests to produce similar dynamic-pressure ratios. The very good agreement in the plots of the outer limit of the water spray for the two tests presented in figure 8(c) indicates that the local dynamic pressure – not the Mach number – is the dominant factor influencing the penetration of the water spray.

Single-Orifice Injection

Figure 8(d) shows plots from the three tests with single-orifice nozzles. The upper two plots compare the effects of the dynamic-pressure ratio on penetration with a constant orifice diameter of 0.076 cm. The top and bottom plots show the effect of orifice diameter (0.076 cm and 0.178 cm) on penetration at about the same dynamic-pressure ratio.

Penetration Correlation

Single-orifice injection.- The authors of reference 12 developed an equation for predicting the outer limit of the water spray for injection through a single orifice normal to a flat plate in a hypersonic airstream. The dynamic-pressure ratio (ratio of jet dynamic pressure to free-stream dynamic pressure) was found to be the only dynamic factor in the equation. This equation was used to compute the outer limit of the water spray for the three tests with single-orifice injection. The dynamic pressure of the airstream at the injection site in the flow field was used in this computation in place of the free-stream dynamic pressure. The injection-site dynamic pressure $\left(\frac{1}{2}\rho_L V_L^2\right)$ was about one-half the free-stream dynamic pressure, and the local static pressure was about one-fifth the free-stream dynamic pressure.

The comparisons of the measured outer limit of the water spray with that predicted by the equation of reference 12 are shown in figure 9. The computations and measurements were made relative to the model surface, but the comparison plots are in the

x,y coordinate system of figure 6. The good agreement indicates that this equation may be used to predict the outer limit of the water spray for single-orifice injection in the flow field of a body if the dynamic-pressure ratio is based on flow conditions at the injection site.

Multiple-orifice injection.- The injection from the multiple-orifice nozzles is complicated by the possible interaction of jets within a cluster and, in some cases, by interaction of jets between clusters as seen in the shielding effect. Each nozzle probably has its own injection characteristics, and a single equation to describe the coordinates of the outer limit of the water spray would be very complex. The injection appears to be basically two-phased. In the initial phase the water acts like a coherent jet, and in the second phase it is broken up by the airstream and is swept downstream in a spraylike condition. The spray, in most cases, reaches a maximum distance from the model surface and then remains essentially parallel to the surface.

These observations suggested that the maximum penetrations could be related to the dynamic factor which influences initial jet penetration. The equation of the initial coherent jet is presented in the appendix, and from the manipulation of this equation, the dynamic factor is found to have the form of the square root of the local dynamic-pressure ratio. In figure 10 the maximum spray penetration is plotted against this parameter for the tests with nozzles A and C. Note that the local dynamic pressure at the injection site is used. These data are limited, but there appears to be a trend toward good correlation for the case of no shielding (nozzle A) and shielding (nozzle C). The shielding effect results in penetration which is about twice that for the case of no shielding.

CONCLUDING REMARKS

Water was injected through single- and multiple-orifice nozzles from the sides of a 0.375-scale model of the RAM C spacecraft. The basic data are presented in the form of photographs and plots of the outer limit of the water spray.

The measured coordinates of the outer limit of the water spray for the tests with the single-orifice injection are in good agreement with those computed by an equation derived by Catton, Hill, and McRae (AIAA Journal, vol. 6, no. 11, 1968). The dynamic pressure of the airstream at the injection site was used in the computation.

By manipulation of the equation of motion of a coherent jet in its initial state, it was shown in the appendix that the initial penetration is proportional to the square root of the local dynamic-pressure ratio. The square root of the local dynamic-pressure ratio is shown to correlate the maximum water spray penetration for injection from the multiple-orifice nozzles.

The penetration for some of the jets from a multiple-orifice nozzle in which some jets were alined directly behind other jets was significantly increased due to an apparent shielding produced by the forward jets.

Langley Research Center,
National Aeronautics and Space Administration,
Langley Station, Hampton, Va., January 15, 1970.

APPENDIX

EQUATION OF A COHERENT JET IN ITS INITIAL STATE

The purpose of this appendix is to show that the dynamic factor which influences the behavior of a coherent jet in its initial state (very near the injection site) is the square root of the dynamic-pressure ratio at the injection site. The coordinate system employed (fig. 6) has its origin at the injection site; x' is parallel to the model surface and y' is in the direction of initial injection.

The y'-position of a unit section of the jet is given by

$$y' = V_j t \tag{1}$$

The aerodynamic force $F_{x'}$ acting on a section of the jet of unit length L_j along the x'-axis is

$$F_{x'} = C_D D_j L_j q_L \tag{2}$$

where

$$q_L = \frac{1}{2} \rho_L V_L^2$$

Now, by writing the mass of the section of the jet as

$$\frac{\pi}{4} \rho_j D_j^2 L_j$$

the acceleration $\ddot{x}'$ can be written

$$\ddot{x}' = \frac{2 C_D \rho_L V_L^2}{\pi D_j \rho_j} \tag{3}$$

Assuming constant acceleration and integrating equation (3) twice with respect to time results in

$$x' = \frac{C_D \rho_L V_L^2}{\pi D_j \rho_j} t^2 \tag{4}$$

Now eliminating time between equations (1) and (4) and solving for y' gives

$$y' = \sqrt{\frac{\pi D_j x'}{C_D}} \sqrt{\frac{\rho_j V_j^2}{\rho_L V_L^2}} \tag{5}$$

Thus, the initial penetration of the jet is proportional to the square root of the local dynamic-pressure ratio.

REFERENCES

1. Cuddihy, William F.; Beckwith, Ivan E.; and Schroeder, Lyle C. (With appendix A by Ivan E. Beckwith, Dennis M. Bushnell, and James L. Hunt; appendix B by Ivan E. Beckwith and Sadie P. Livingston; and appendix C by Ivan E. Beckwith): Flight Test and Analysis of a Method for Reducing Radio Attenuation During Hypersonic Flight. NASA TM X-1331, 1967.

2. Akey, Norman D.; and Cross, Aubrey E. (With appendix A by Thomas G. Campbell, appendix B by Fred B. Beck, and appendix C by W. Linwood Jones, Jr.): Radio Blackout Alleviation and Plasma Diagnostic Results From a 25 000 Foot Per Second Blunt-Body Reentry. NASA TN D-5615, 1970.

3. Beckwith, Ivan E.; Bushnell, Dennis M.; and Huffman, Jarrett K.: Investigation of Water Injection on Models of Gemini Vehicle and Resulting Predictions for GT-3 Reentry Communications Experiment. NASA TM X-1200, 1966.

4. Beckwith, Ivan E.; and Huffman, Jarrett K.: Injection and Distribution of Liquids in the Flow Fields of Blunt Shapes at Hypersonic Speeds. NASA TM X-989, 1964.

5. Ingebo, Robert D.; and Foster, Hampton, H.: Drop-Size Distribution for Crosscurrent Breakup of Liquid Jets in Airstreams. NACA TN 4087, 1957.

6. Weiss, Malcolm A.; and Worsham, Charles H.: Atomization in High Velocity Airstreams. ARS J., vol. 29, no. 4, Apr. 1959, pp. 252-259.

7. Bitron, Moshe D.: Atomization of Liquids by Supersonic Air Jets. Ind. Eng. Chem., vol. 47, no. 1, 1955, pp. 23-28.

8. Chelko, Louis J.: Penetration of Liquid Jets Into a High-Velocity Air Stream. NACA RM E50F21, 1950.

9. Ingebo, Robert D.: Study of Pressure Effects on Vaporization Rate of Drops in Gas Streams. NACA TN 2850, 1953.

10. Shapiro, A. H.; Wadleigh, K. R.; Gavril, B. D.; and Fowle, A. A.: The Aerothermopressor – A Device for Improving the Performance of a Gas-Turbine Power Plant. Trans. ASME, vol. 78, no. 3, Apr. 1956, pp. 617-653.

11. Emmons, Howard W., ed.: Fundamentals of Gas Dynamics. Vol. III of High Speed Aerodynamics and Jet Propulsion. Princeton Univ. Press, c.1958.

12. Catton, I.; Hill, D. E.; and McRae, R. P.: Study of Liquid Jet Penetration in a Hypersonic Stream. AIAA J., vol. 6, no. 11, Nov. 1968, pp. 2084-2089.

TABLE I.- TEST CONDITIONS AND PENETRATION PARAMETERS

Figure	Nozzle	Tunnel conditions				Penetration parameters						
		p_t, MN/m^2	T_t, ^oK	M_∞	q_∞, kN/m^2	p_w, MN/m^2	V_j, m/sec	$\frac{\rho_j V_j}{\rho_\infty V_\infty}$	$\frac{\rho_j V_j^2}{\rho_\infty V_\infty^2}$	$\frac{\rho_j V_j}{\rho_L V_L}$	$\frac{\rho_j V_j^2}{\rho_L V_L^2}$	$\frac{m_j}{m_B}$
7(a)	A	5.96	1094	7.26	39.3	1.19	35.98	646	16.40	924	31.3	1.5
7(b)	C	5.96	1067	7.26	39.4	1.19	35.98	636	16.00	901	30.6	---
7(c)	A	12.51	1062	7.26	83.4	1.46	39.94	334	9.55	478	18.1	0.8
7(d)	C	13.03	1072	7.26	86.3	1.28	37.31	301	8.00	430	15.3	5.0
7(e)	C	6.03	1028	7.26	39.6	2.00	46.72	830	29.00	1187	55.4	13.7
7(f)	C	13.55	1111	10.57	16.1	0.86	30.78	1400	29.70	1960	56.7	23.0
7(g)	C	2.89	978	7.26	19.3	0.88	30.78	1064	24.5	1522	46.8	17.6
7(h)	B	2.94	1044	7.26	19.6	0.90	31.40	1110	25.1	1587	47.9	6.6
7(i)	C	12.99	1100	7.26	85.6	1.46	39.94	331	9.3	473	17.8	5.5
7(j)	B	12.96	1133	7.26	85.5	1.46	39.94	331	9.3	473	17.8	2.0
7(k)	A	0.85	861	7.26	5.9	0.43	21.64	2319	40.0	3316	76.4	5.5
7(ℓ)	C	0.85	856	7.26	5.9	0.41	21.34	2287	38.8	3270	73.7	37.8
7(m)	A	3.65	1108	10.37	4.7	0.43	21.64	3382	50.0	4735	95.5	7.8
7(n)	C	3.17	1064	10.37	4.1	0.41	21.34	3733	55.8	5226	106.6	60.0
7(o)	D	0.85	1007	7.26	5.7	0.43	21.64	2591	41.3	3617	78.9	---
7(p)	D	0.85	1007	7.26	5.7	0.84	30.18	3613	79.0	5167	150.1	---
7(q)	E	0.86	897	7.26	5.9	0.42	21.34	2336	38.8	----	74.1	---

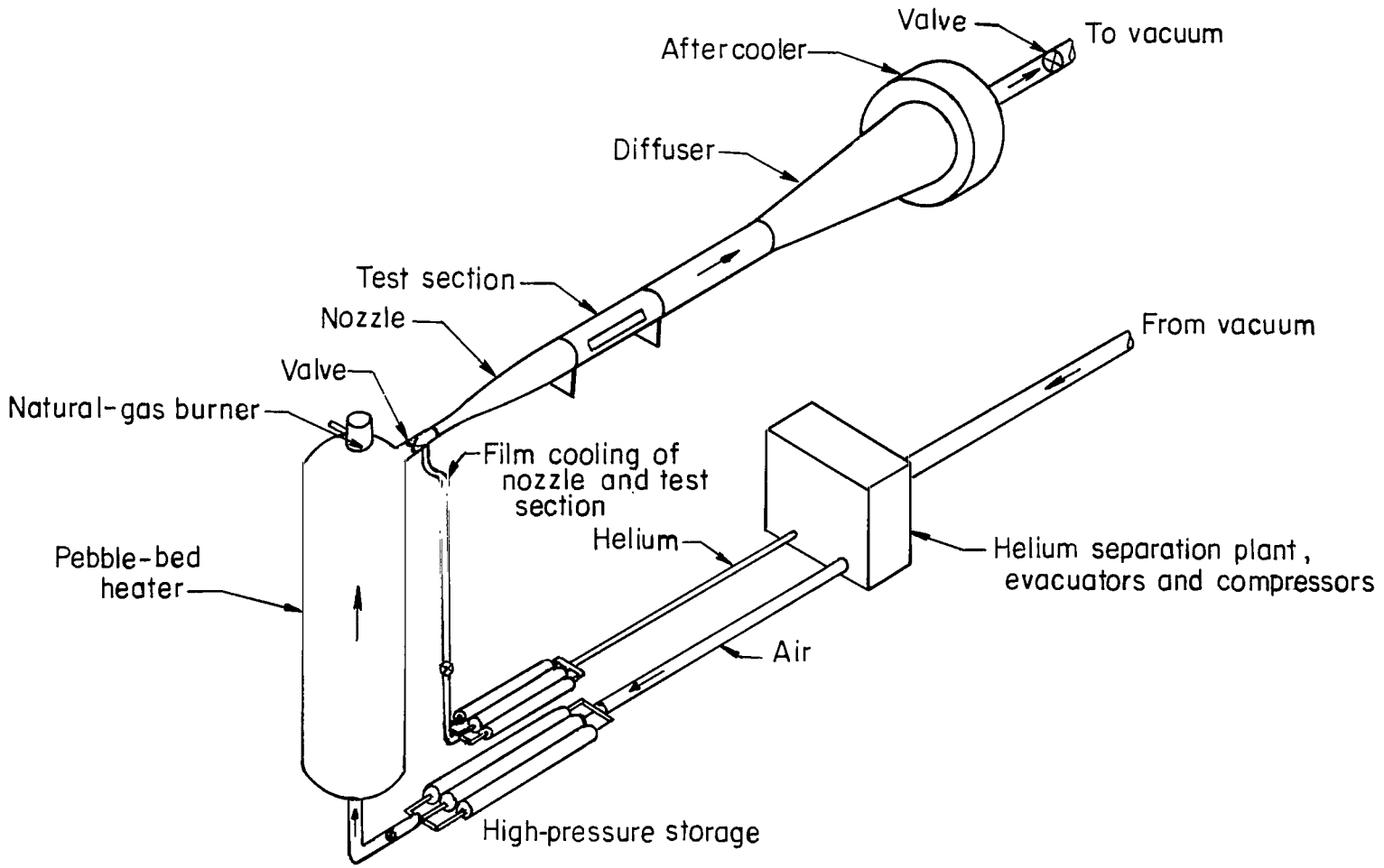

Figure 1.- Diagram of Ames 3.5-foot hypersonic wind tunnel.

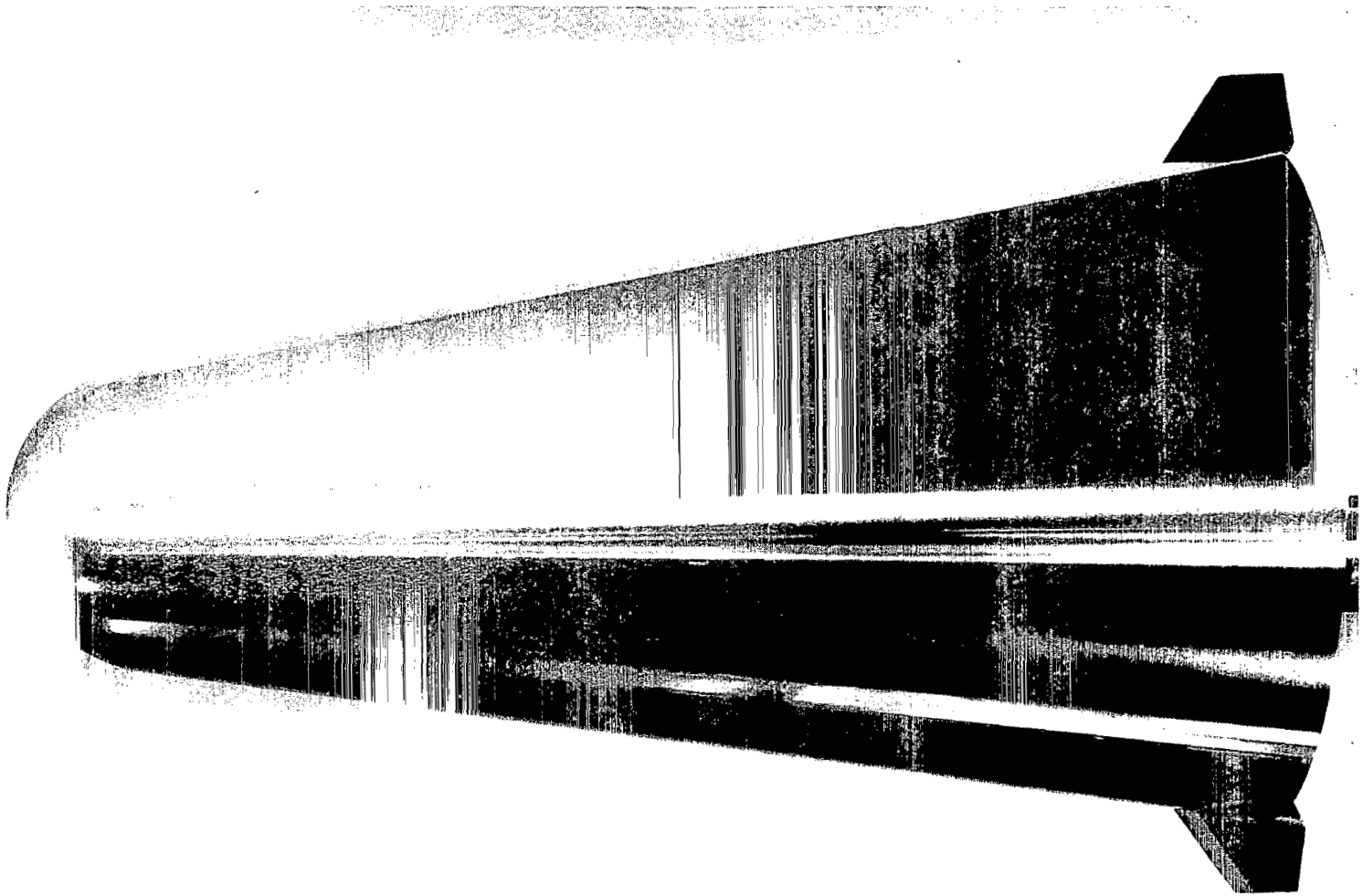

Figure 2.- Plan view of 0.375-scale model of RAM C spacecraft.

L-70-1510

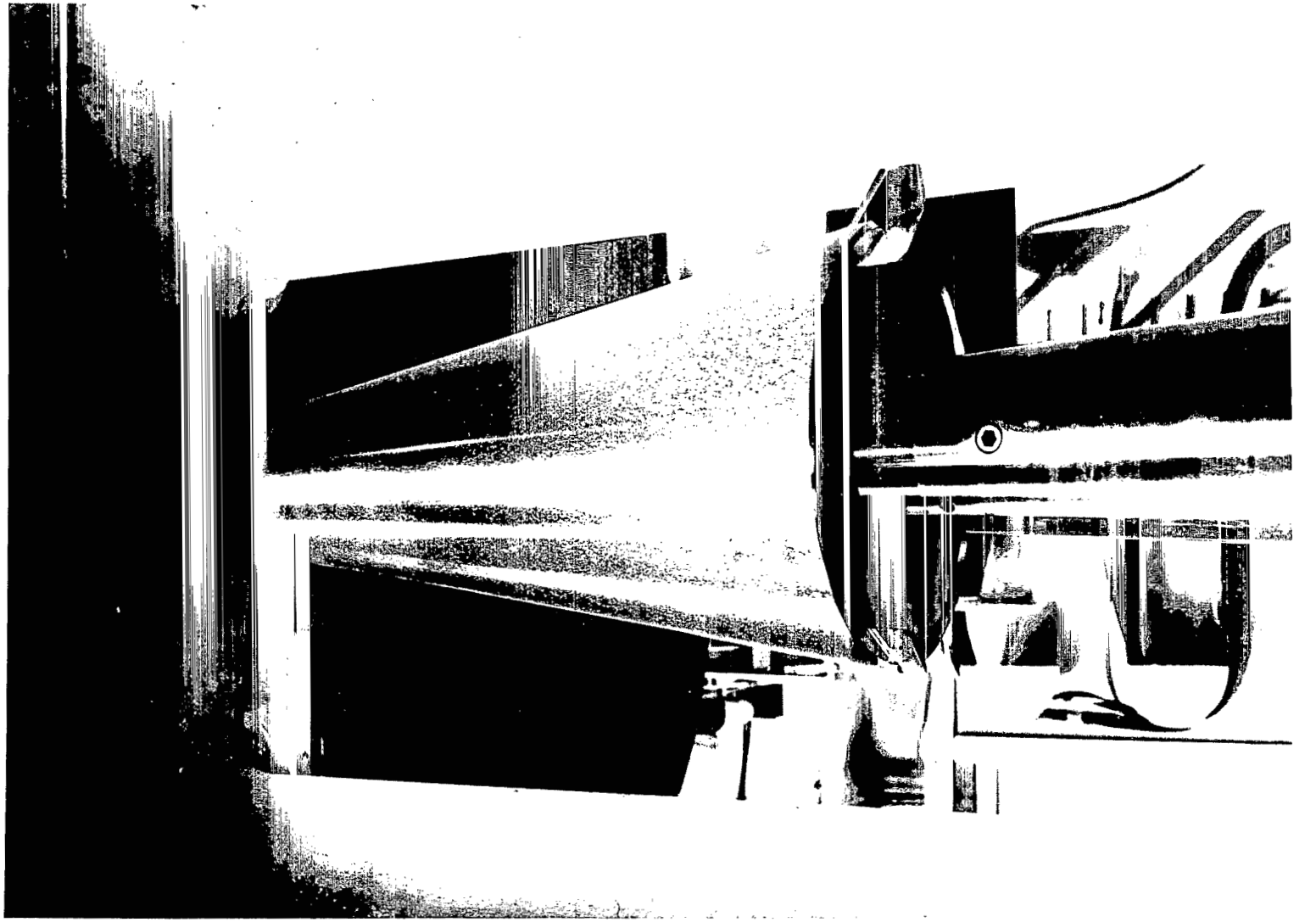

Figure 3.- Photograph of 0.375-scale model of RAM C spacecraft mounted in Ames 3.5-foot hypersonic wind tunnel. L-70-1511

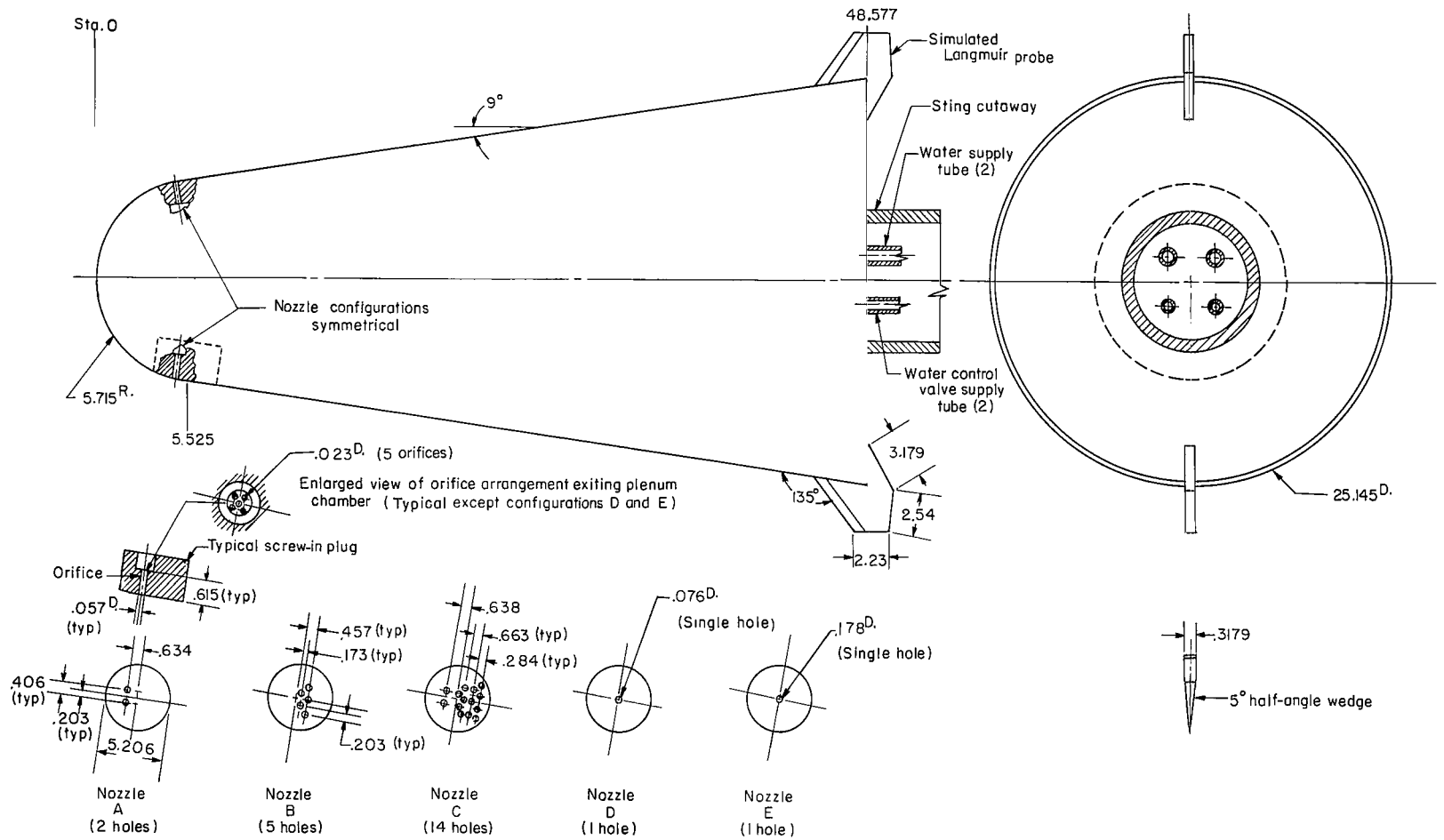

Figure 4.- Schematic of model and nozzle configurations. All dimensions are in centimeters unless indicated otherwise.

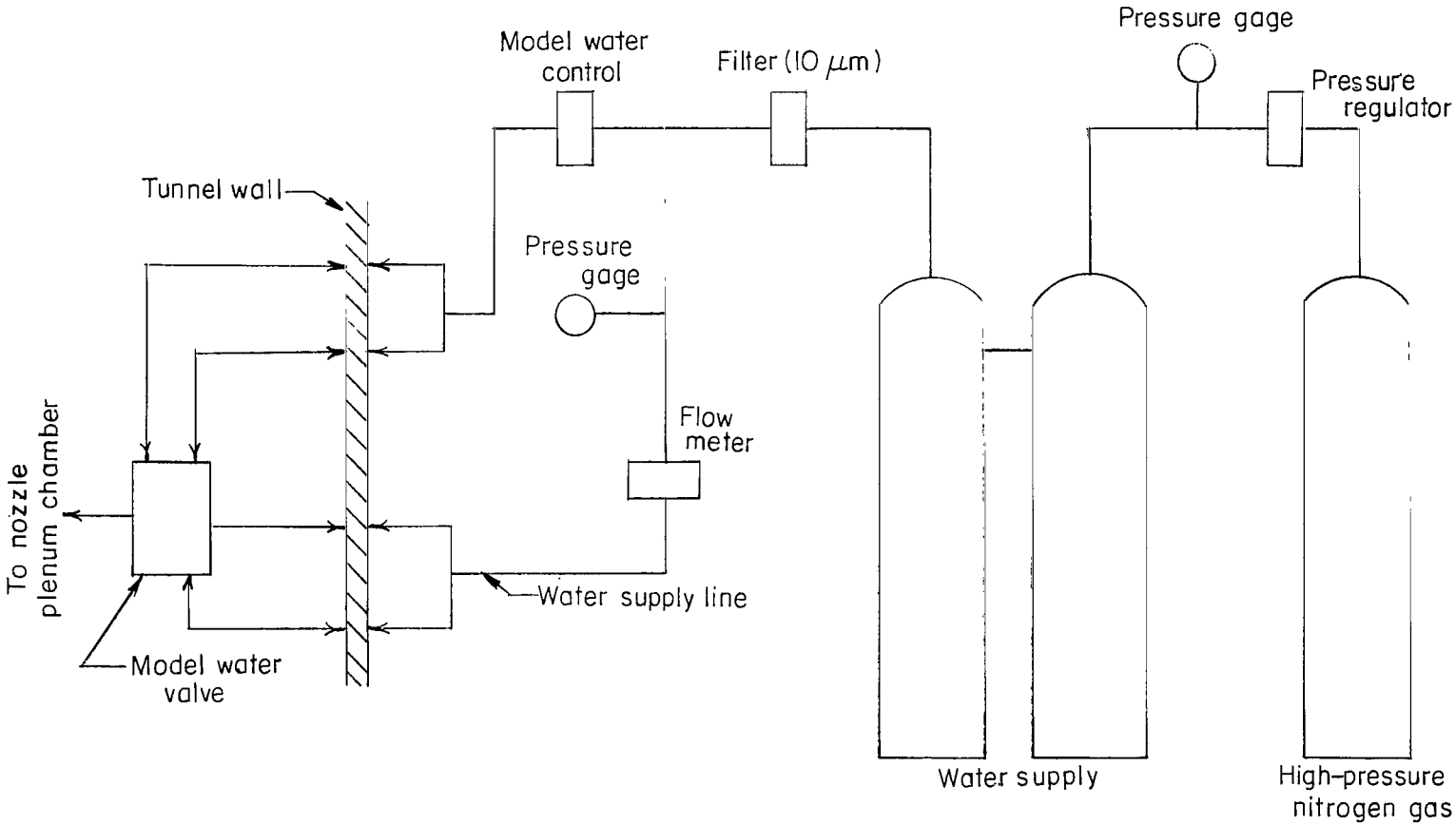

Figure 5.- Schematic of water-injection system.

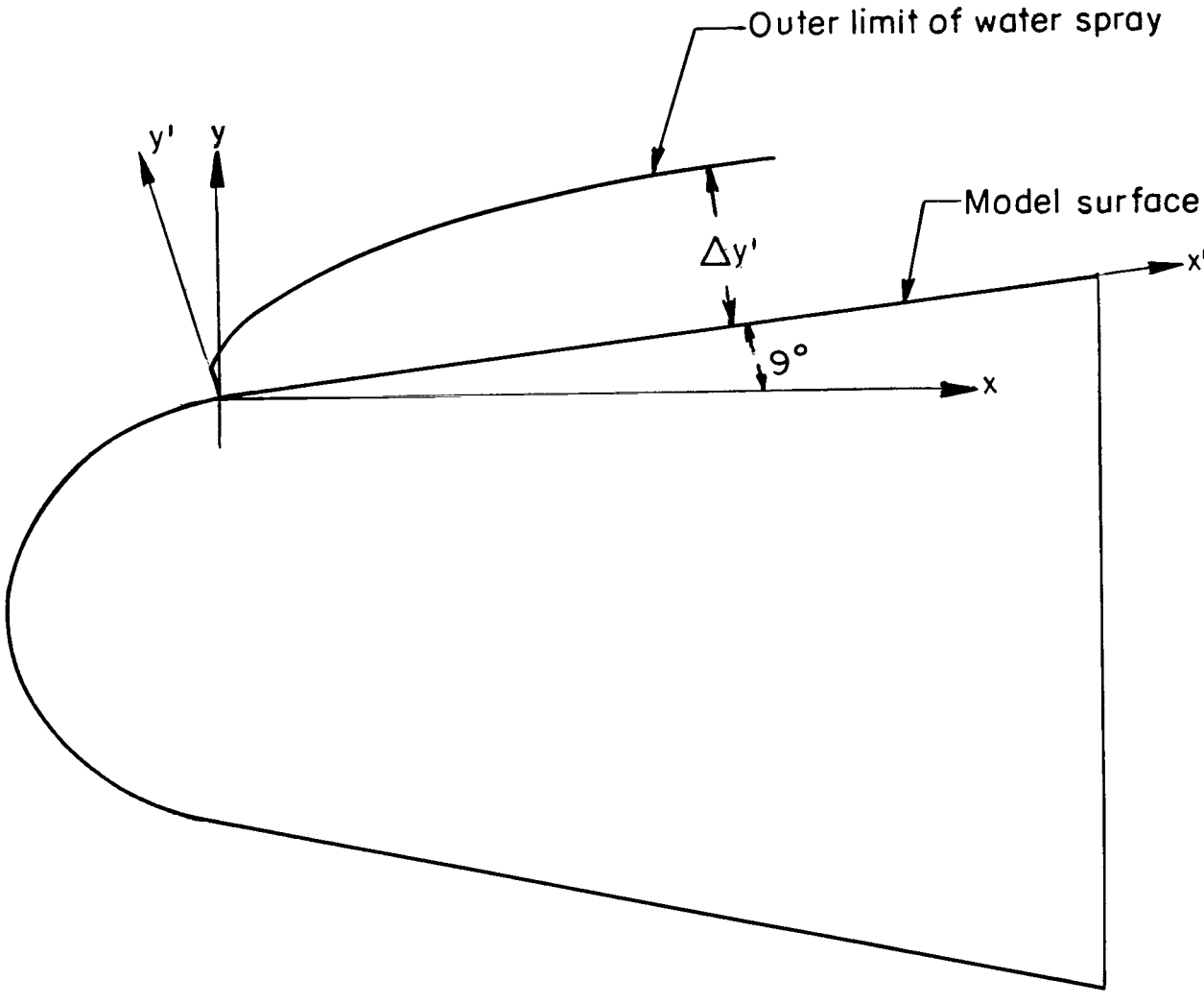

Figure 6.- Coordinate system and penetration terms.

See figure 8 (a)

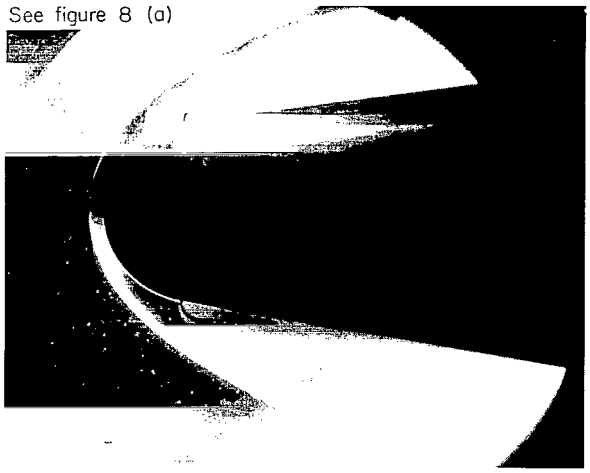

(a) Nozzle A; $M_\infty = 7.26$; $V_j = 35.98$ m/sec; $\frac{\rho_j V_j^2}{\rho_L V_L^2} = 31.3$; $\frac{m_j}{m_B} = 1.5$.

See figure 8 (a)

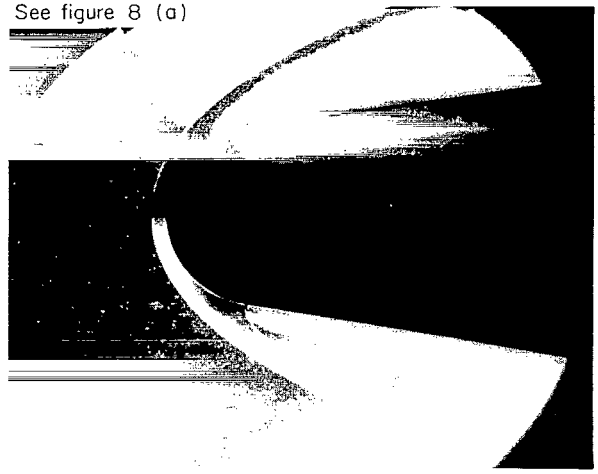

(c) Nozzle A; $M_\infty = 7.26$; $V_j = 39.94$ m/sec; $\frac{\rho_j V_j^2}{\rho_L V_L^2} = 18.1$; $\frac{m_j}{m_B} = 0.8$.

See figure 8 (a)

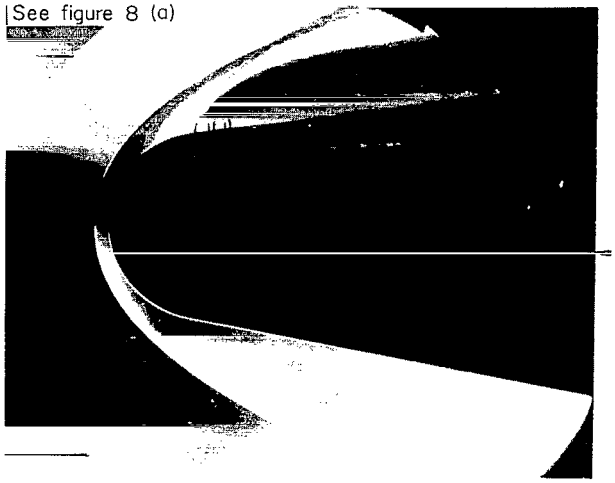

L-70-1504

(b) Nozzle C (orifices on one side only); $M_\infty = 7.26$; $V_j = 35.98$ m/sec; $\frac{\rho_j V_j^2}{\rho_L V_L^2} = 30.6$.

Figure 7.- Schlieren photographs showing outer limits of water spray along with pertinent test conditions.

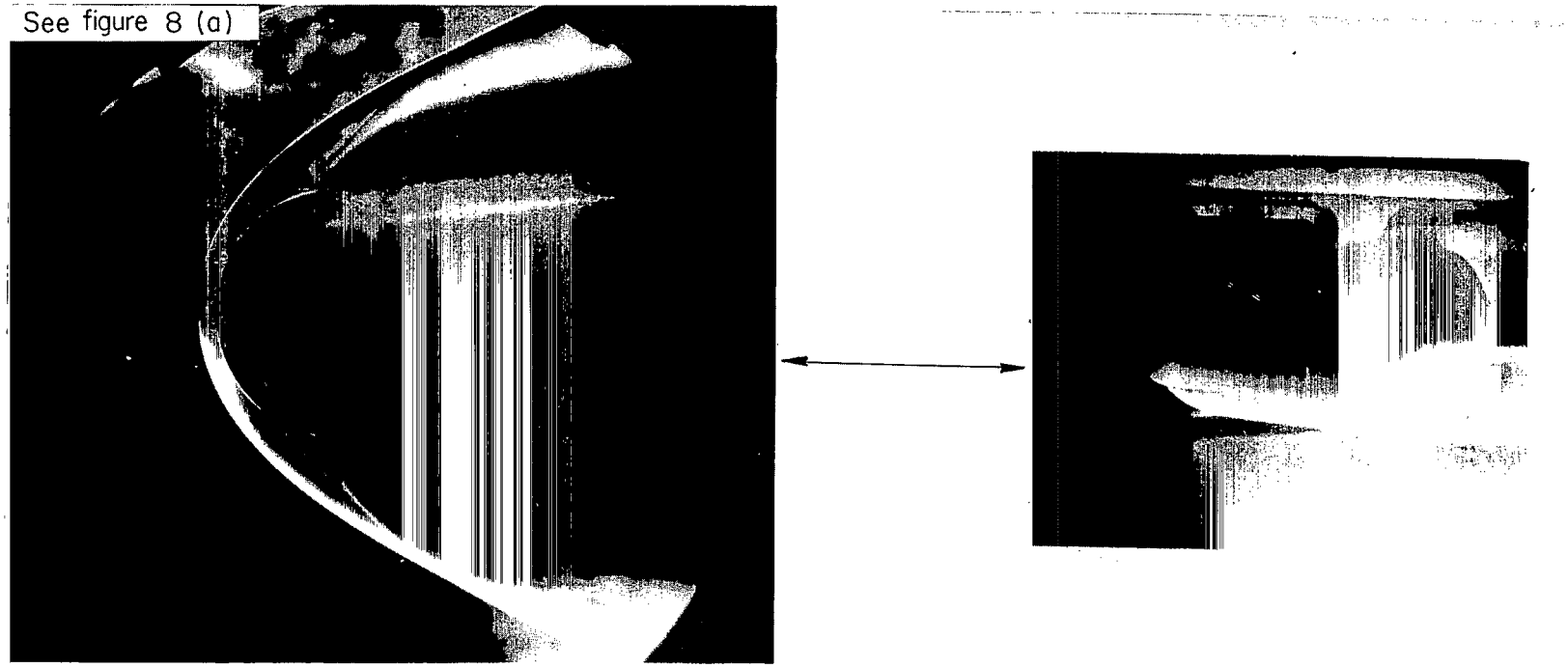

(d) Nozzle C; $M_\infty = 7.26$; $V_j = 37.31$ m/sec; $\frac{\rho_j V_j^2}{\rho_L V_L^2} = 15.3$; $\frac{m_j}{m_B} = 5.0$.

Figure 7.- Continued.

L-70-1505

See figure 8 (c)

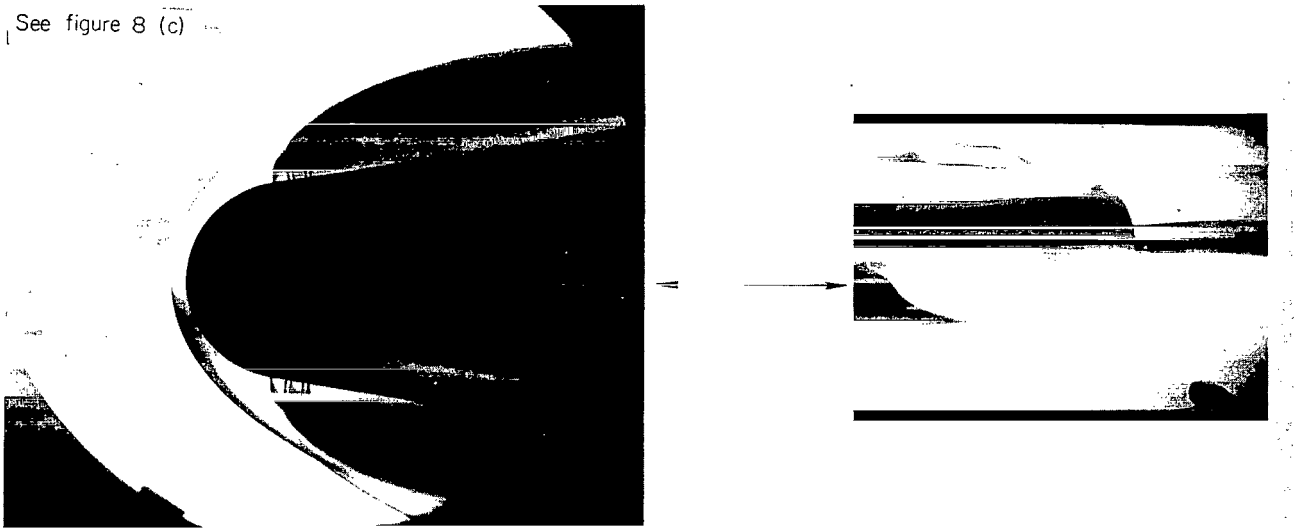

(e) Nozzle C; $M_\infty = 7.26$; $V_j = 46.72$ m/sec; $\frac{\rho_j V_j^2}{\rho_L V_L^2} = 55.4$; $\frac{m_j}{m_B} = 13.7$.

See figure 8 (c)

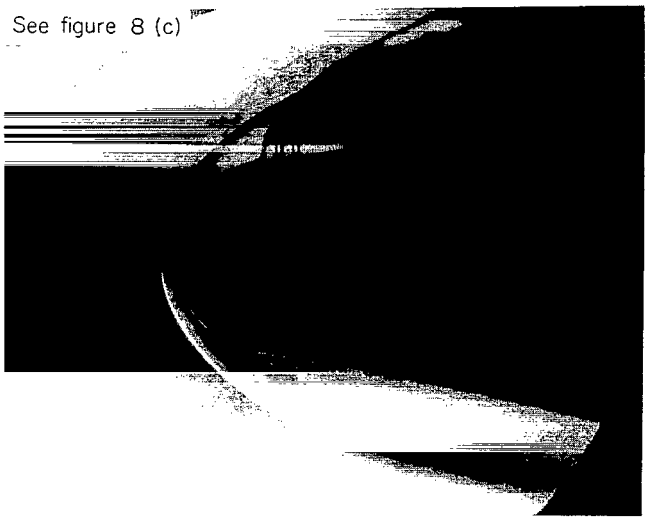

(f) Nozzle C; $M_\infty = 10.57$; $V_j = 30.78$ m/sec; $\frac{\rho_j V_j^2}{\rho_L V_L^2} = 56.7$; $\frac{m_j}{m_B} = 23.0$.

Figure 7.- Continued.

L-70-1506

(g) Nozzle C; $M_\infty = 7.26$; $V_j = 30.78$ m/sec;

$$\frac{\rho_j V_j^2}{\rho_L V_L^2} = 46.8; \quad \frac{m_j}{m_B} = 17.6.$$

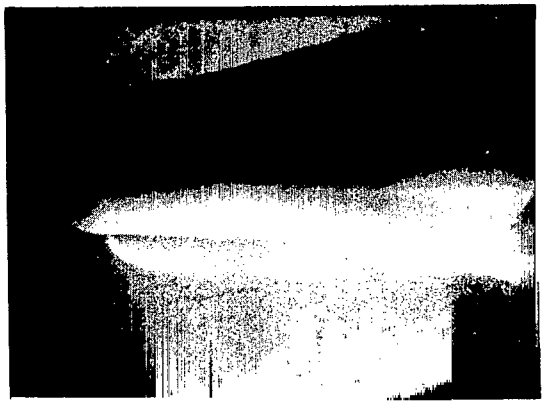

(h) Nozzle B; $M_\infty = 7.26$; $V_j = 31.40$ m/sec;

$$\frac{\rho_j V_j^2}{\rho_L V_L^2} = 47.9; \quad \frac{m_j}{m_B} = 6.6.$$

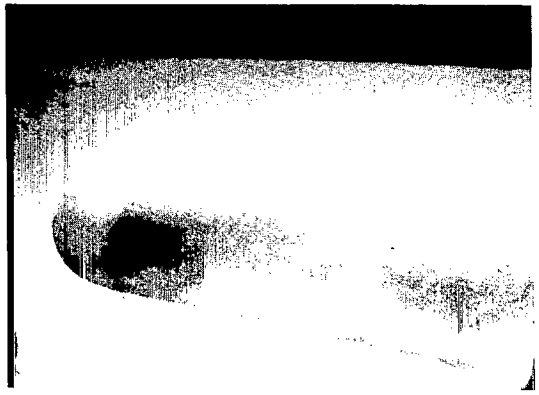

(i) Nozzle C; $M_\infty = 7.26$; $V_j = 39.94$ m/sec;

$$\frac{\rho_j V_j^2}{\rho_L V_L^2} = 17.8; \quad \frac{m_j}{m_B} = 5.5.$$

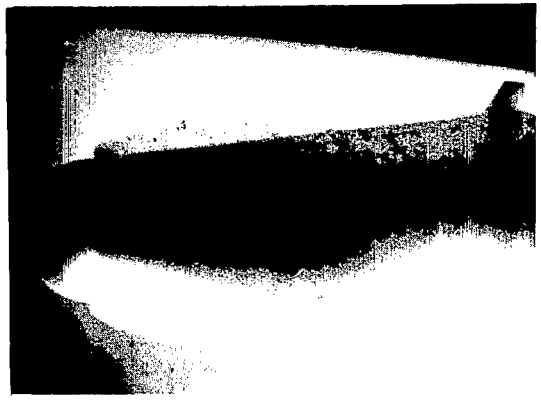

(j) Nozzle B; $M_\infty = 7.26$; $V_j = 39.94$ m/sec;

$$\frac{\rho_j V_j^2}{\rho_L V_L^2} = 17.8; \quad \frac{m_j}{m_B} = 2.0.$$

Figure 7.- Continued.

L-70-1507

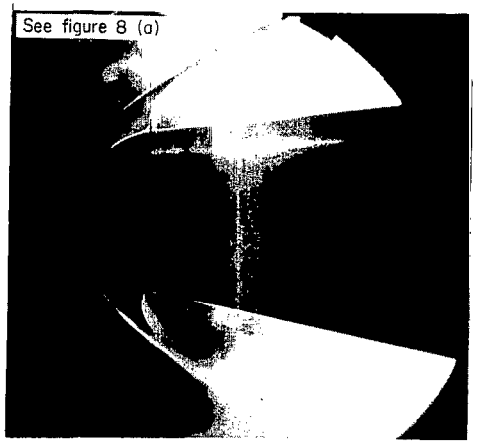

(k) Nozzle A; $M_\infty = 7.26$; $V_j = 21.64$ m/sec; $\frac{\rho_j V_j^2}{\rho_L V_L^2} = 76.4$; $\frac{m_j}{m_B} = 5.5$.

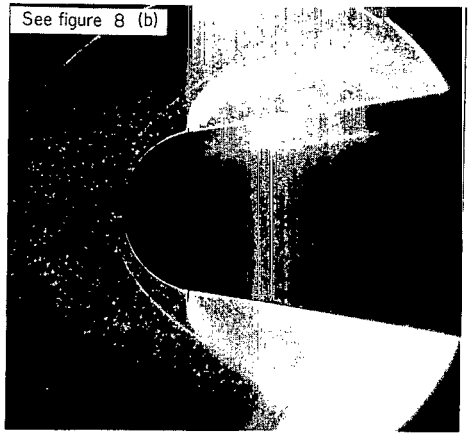

(m) Nozzle A; $M_\infty = 10.37$; $V_j = 21.64$ m/sec; $\frac{\rho_j V_j^2}{\rho_L V_L^2} = 95.5$; $\frac{m_j}{m_B} = 7.8$.

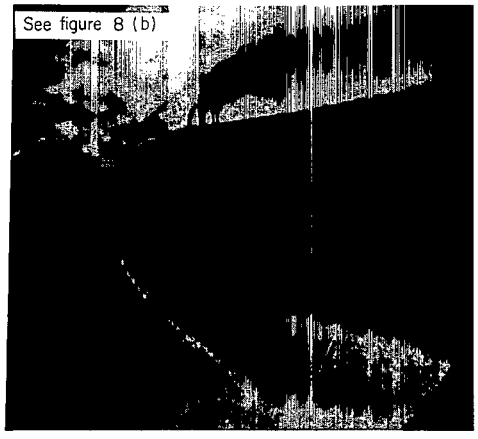

(n) Nozzle C; $M_\infty = 10.37$; $V_j = 21.34$ m/sec; $\frac{\rho_j V_j^2}{\rho_L V_L^2} = 106.6$; $\frac{m_j}{m_B} = 60.0$.

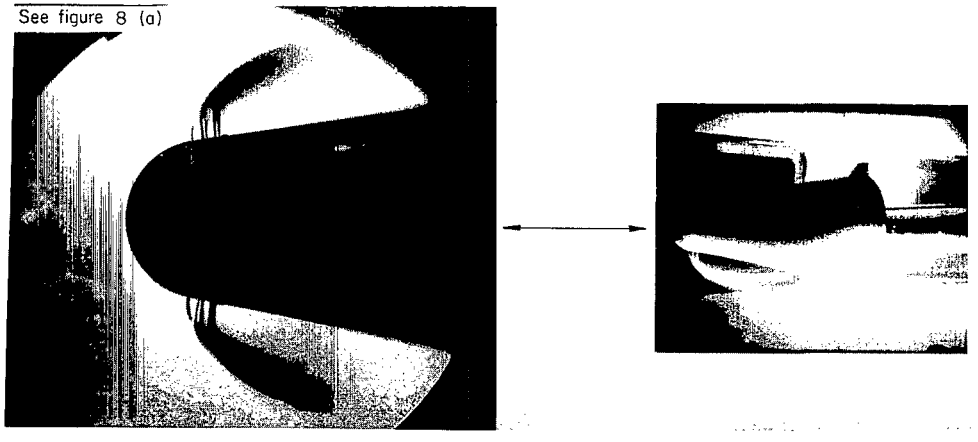

(l) Nozzle C; $M_\infty = 7.26$; $V_j = 21.34$ m/sec; $\frac{\rho_j V_j^2}{\rho_L V_L^2} = 73.7$; $\frac{m_j}{m_B} = 37.8$.

Figure 7.- Continued.

L-70-1508

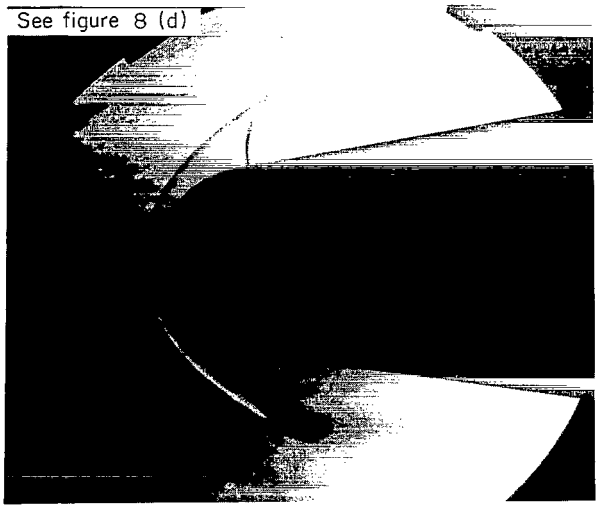

(o) Nozzle D; $M_\infty = 7.26$; $V_j = 21.64$ m/sec; $\frac{\rho_j V_j^2}{\rho_L V_L^2} = 78.9$.

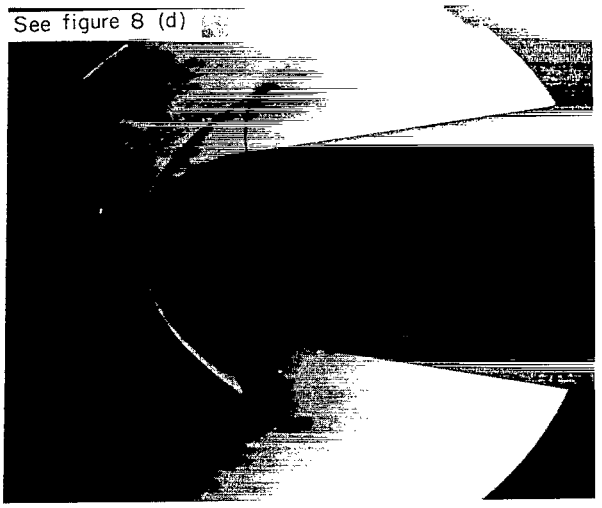

(p) Nozzle D; $M_\infty = 7.26$; $V_j = 30.18$ m/sec; $\frac{\rho_j V_j^2}{\rho_L V_L^2} = 150.1$.

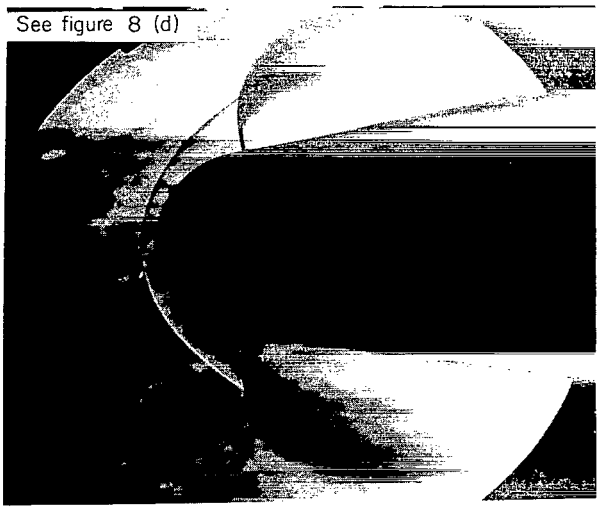

(q) Nozzle E; $M_\infty = 7.26$; $V_j = 21.34$ m/sec; $\frac{\rho_j V_j^2}{\rho_L V_L^2} = 74.1$.

Figure 7.- Concluded.

L-70-1509

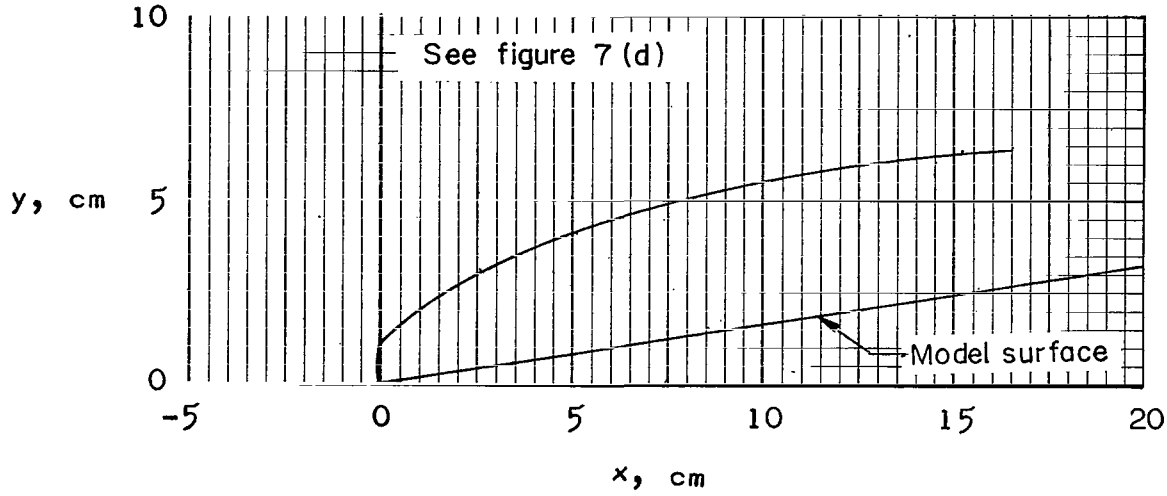

Nozzle C; V_j = 37.31 m/sec ; $\frac{\rho_j V_j^2}{\rho_L V_L^2} = 15.3$

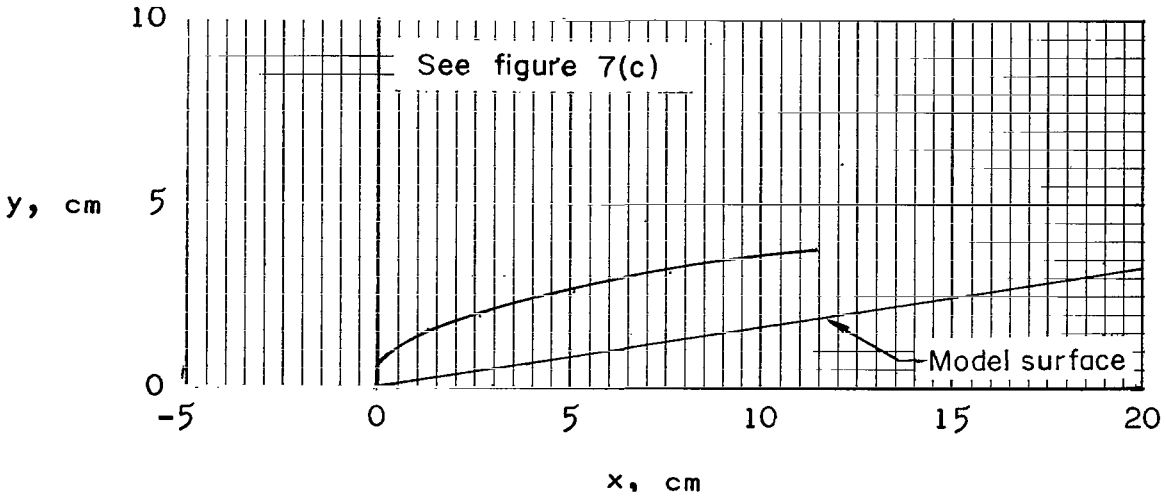

Nozzle A ; V_j = 39.94 m/sec ; $\frac{\rho_j V_j^2}{\rho_L V_L^2} = 18.1$

(a) Comparisons between nozzles A and C at $M_\infty = 7.26$.

Figure 8.- Measured trajectories of outer limit of water spray.

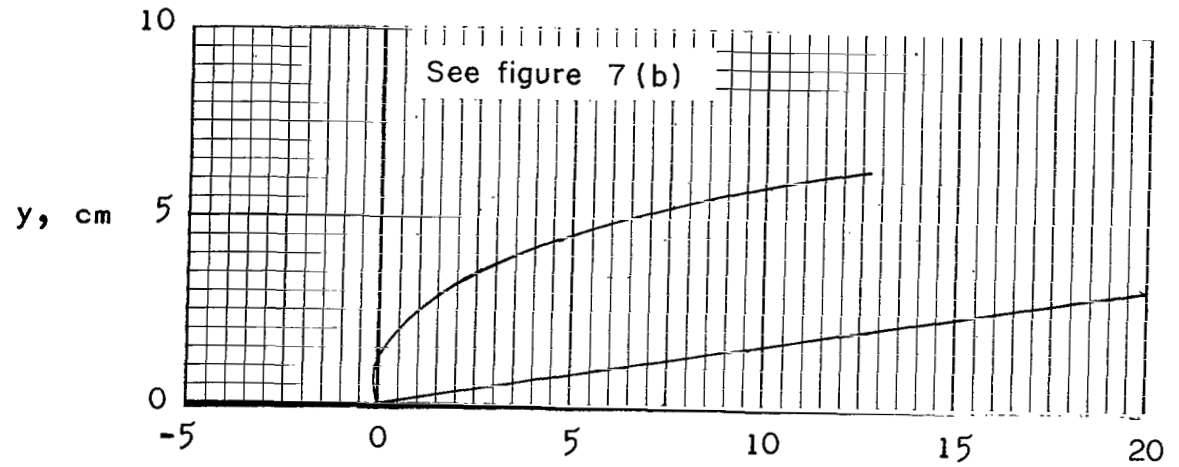

Nozzle C ; V_j = 35.98 m/sec ; $\frac{\rho_j V_j^2}{\rho_L V_L^2}$ = 30.6

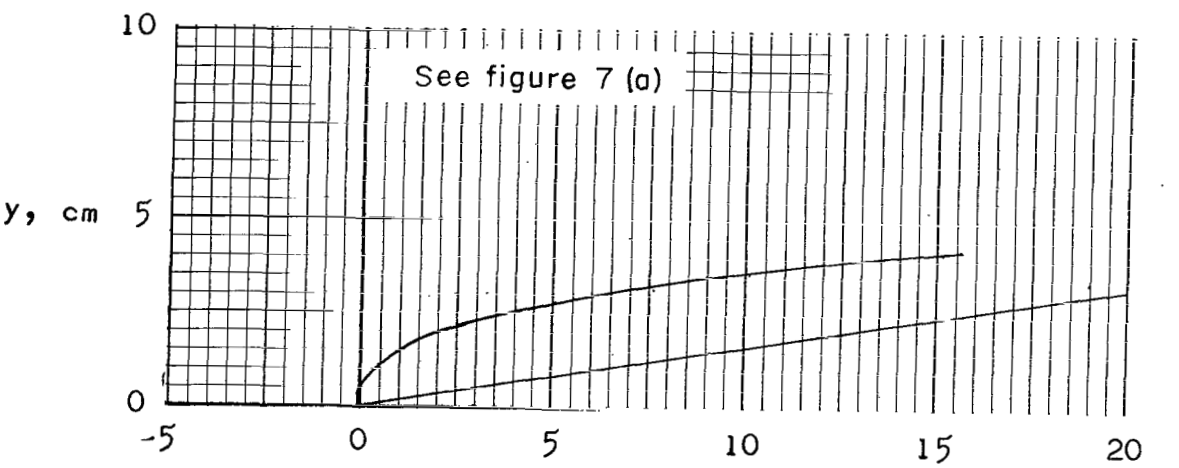

Nozzle A ; V_j = 35.98 m/sec ; $\frac{\rho_j V_j^2}{\rho_L V_L^2}$ = 31.3

(a) Continued.

Figure 8.- Continued.

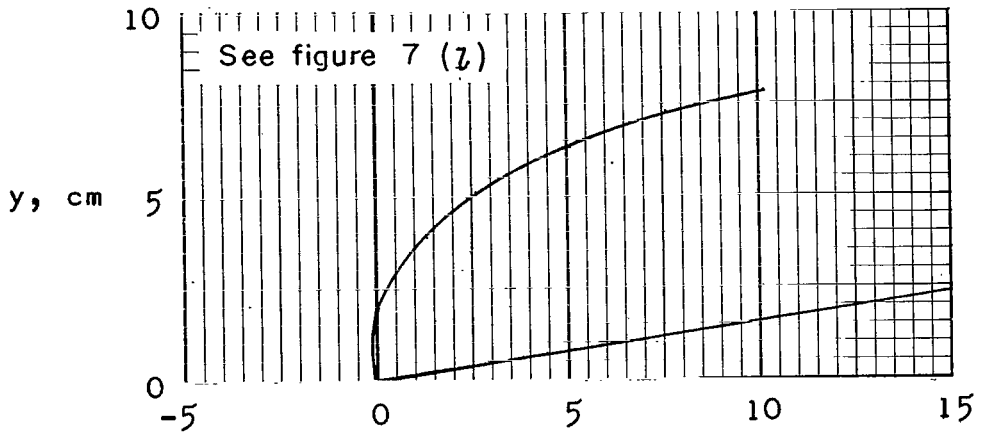

Nozzle C ; V_j = 21.34 m/sec ; $\frac{\rho_j V_j^2}{\rho_L V_L^2}$ = 73.7

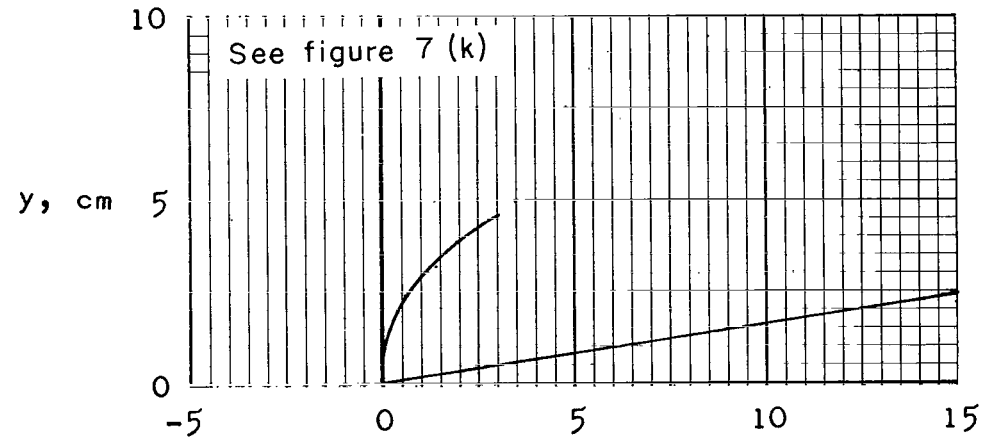

Nozzle A ; V_j = 21.64 m/sec ; $\frac{\rho_j V_j^2}{\rho_L V_L^2}$ = 76.4

(a) Concluded.

Figure 8.- Continued.

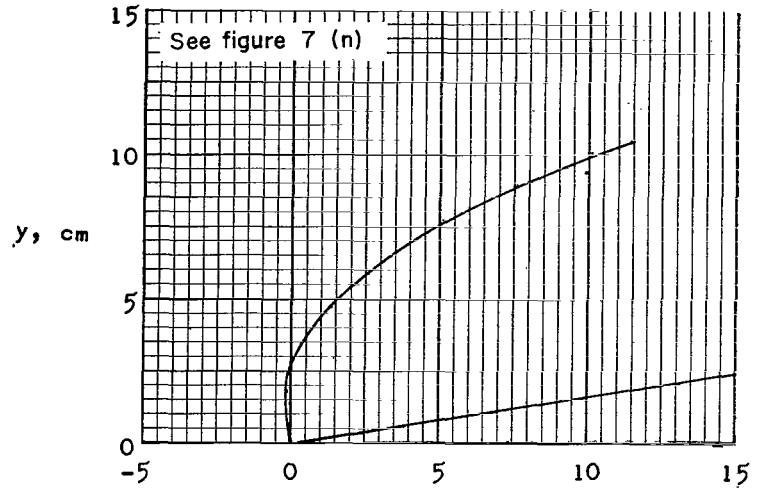

Nozzle C ; V_j = 21.34 m/sec ; $\frac{\rho_j V_j^2}{\rho_L V_L^2} = 106.6$

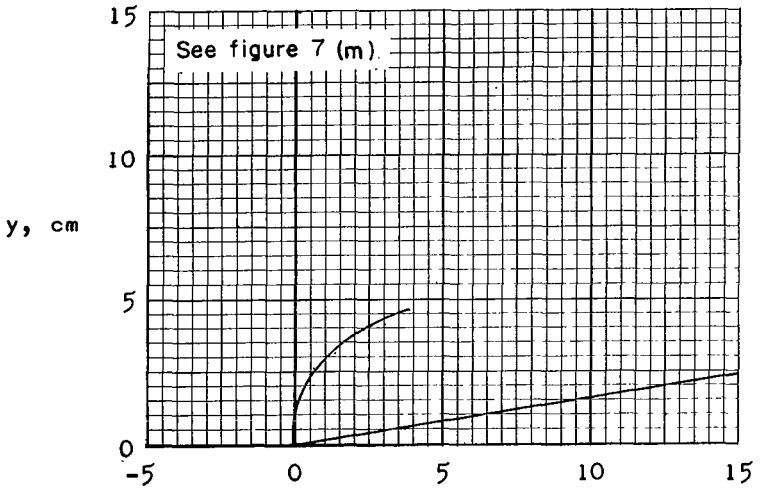

Nozzle A ; V_j = 21.64 m/sec ; $\frac{\rho_j V_j^2}{\rho_L V_L^2} = 95.5$

(b) Comparisons between nozzles A and C at $M_\infty = 10.37$.

Figure 8.- Continued.

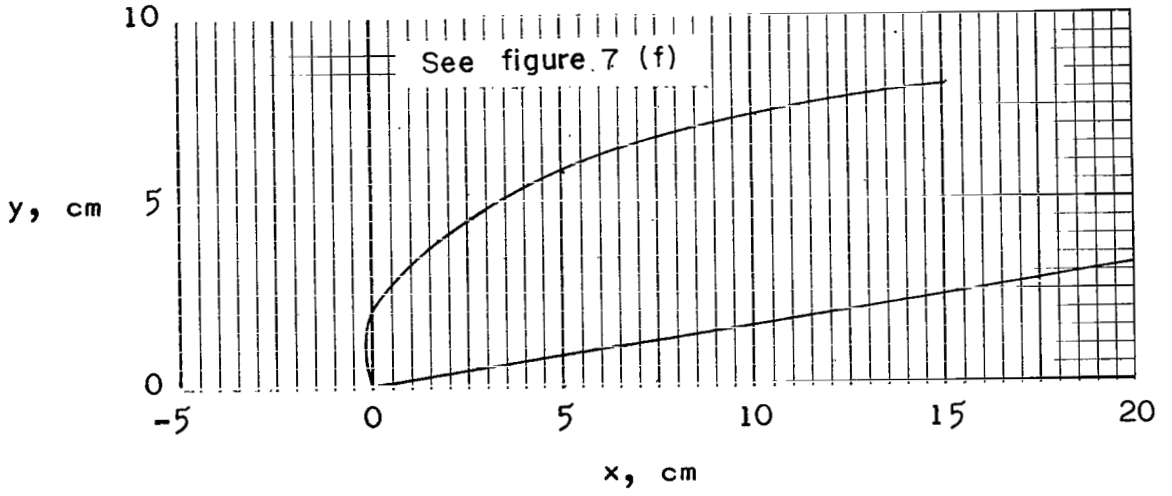

$M_\infty = 10.57$; $V_j = 30.78$ m/sec; $\frac{\rho_j V_j^2}{\rho_L V_L^2} = 56.7$

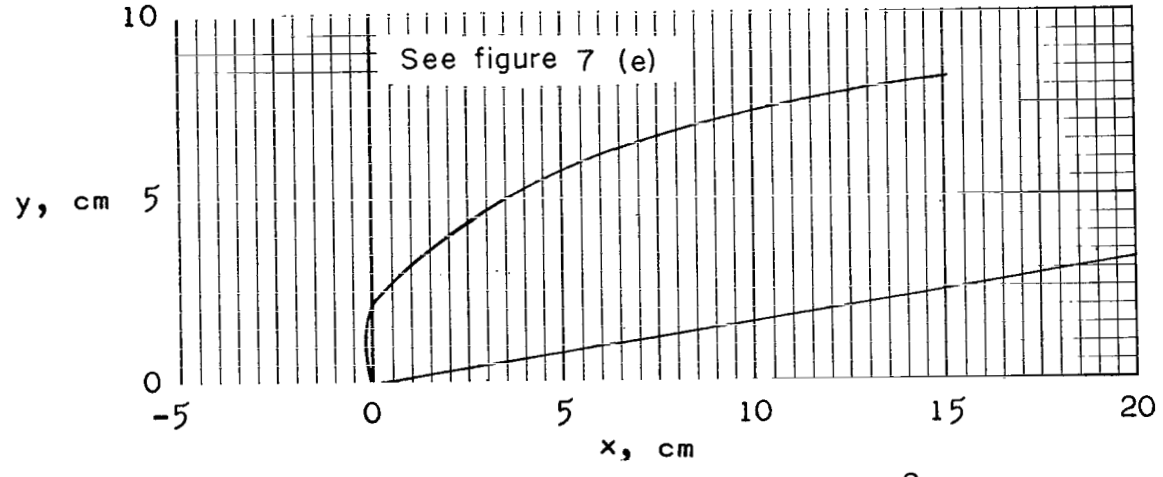

$M_\infty = 7.26$; $V_j = 46.72$ m/sec; $\frac{\rho_j V_j^2}{\rho_L V_L^2} = 55.4$

(c) Comparison of Mach number effect when nozzle C is used.

Figure 8.- Continued.

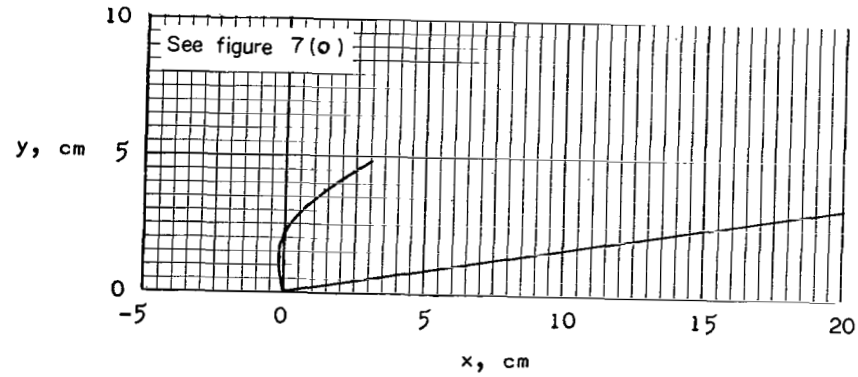

Nozzle D; $V_j = 21.64$ m/sec; $\frac{\rho_j V_j^2}{\rho_L V_L^2} = 78.9$

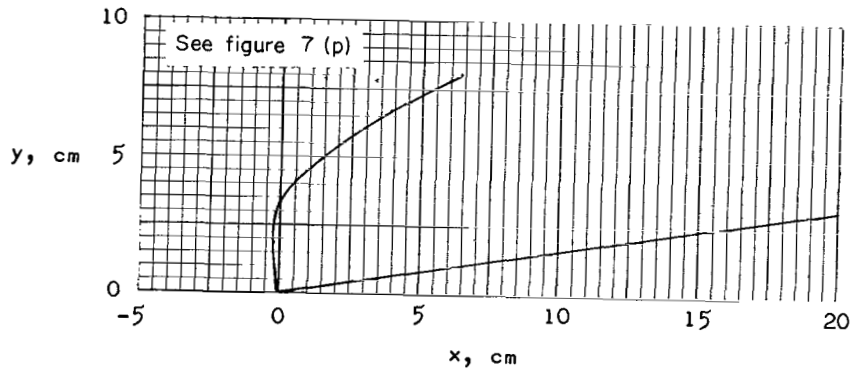

Nozzle D; $V_j = 30.18$ m/sec; $\frac{\rho_j V_j^2}{\rho_L V_L^2} = 150.1$

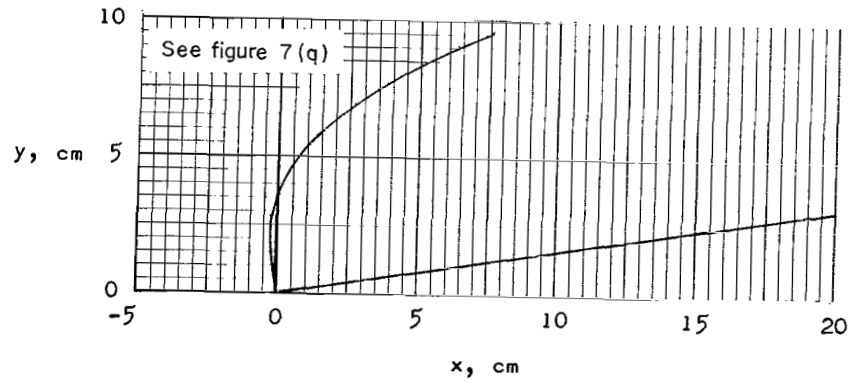

Nozzle E; $V_j = 21.34$ m/sec; $\frac{\rho_j V_j^2}{\rho_L V_L^2} = 74.1$

(d) Single-orifice injection at $M_\infty = 7.26$.

Figure 8.- Concluded.

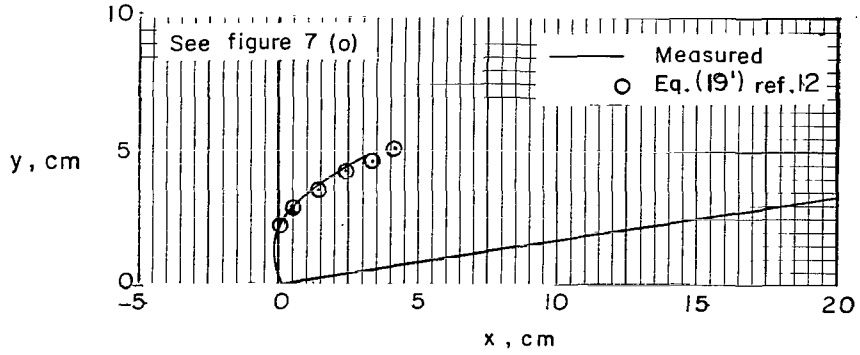

Nozzle D ; $V_j = 21.64$ m/sec ; $\frac{\rho_j V_j^2}{\rho_L V_L^2} = 78.9$

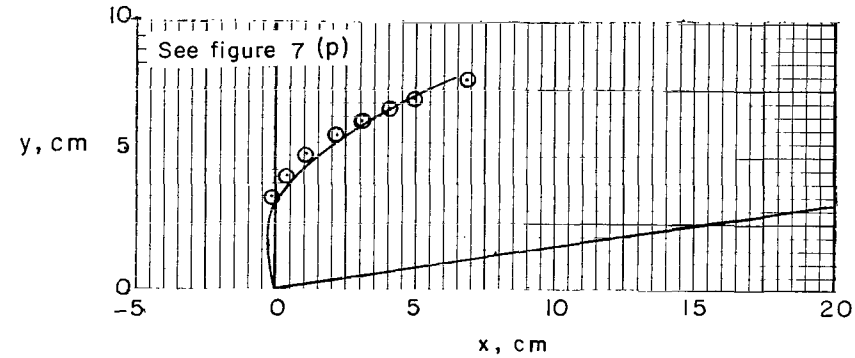

Nozzle D; $V_j = 30.18$ m/sec ; $\frac{\rho_j V_j^2}{\rho_L V_L^2} = 150.1$

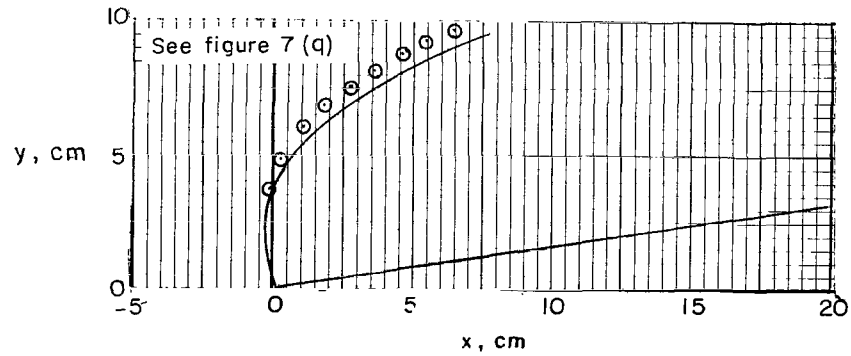

Nozzle E; $V_j = 21.34$ m/sec ; $\frac{\rho_j V_j^2}{\rho_L V_L^2} = 74.1$

Figure 9.- Comparisons of measured and computed water spray trajectories with single-orifice injection.

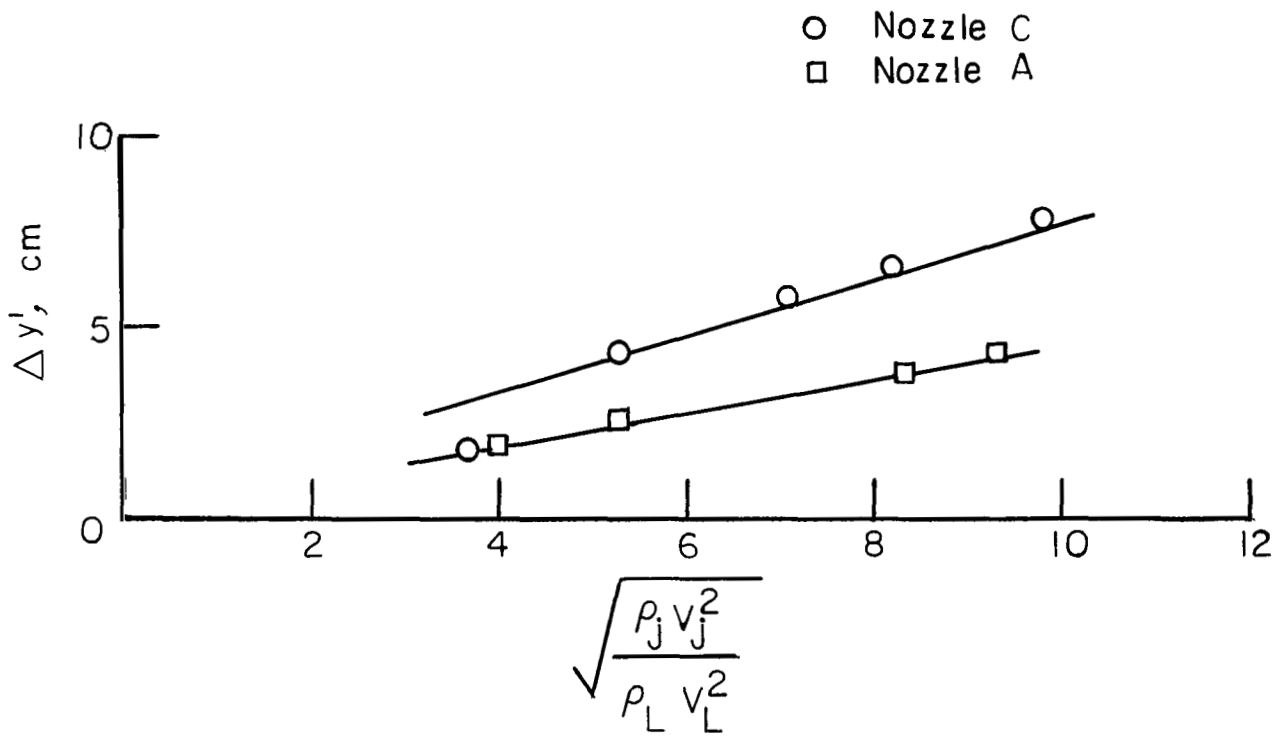

Figure 10.- Maximum spray penetration as a function of correlation parameter.

"The aeronautical and space activities of the United States shall be conducted so as to contribute . . . to the expansion of human knowledge of phenomena in the atmosphere and space. The Administration shall provide for the widest practicable and appropriate dissemination of information concerning its activities and the results thereof."

—NATIONAL AERONAUTICS AND SPACE ACT OF 1958

NASA SCIENTIFIC AND TECHNICAL PUBLICATIONS

TECHNICAL REPORTS: Scientific and technical information considered important, complete, and a lasting contribution to existing knowledge.

TECHNICAL NOTES: Information less broad in scope but nevertheless of importance as a contribution to existing knowledge.

TECHNICAL MEMORANDUMS: Information receiving limited distribution because of preliminary data, security classification, or other reasons.

CONTRACTOR REPORTS: Scientific and technical information generated under a NASA contract or grant and considered an important contribution to existing knowledge.

TECHNICAL TRANSLATIONS: Information published in a foreign language considered to merit NASA distribution in English.

SPECIAL PUBLICATIONS: Information derived from or of value to NASA activities. Publications include conference proceedings, monographs, data compilations, handbooks, sourcebooks, and special bibliographies.

TECHNOLOGY UTILIZATION PUBLICATIONS: Information on technology used by NASA that may be of particular interest in commercial and other non-aerospace applications. Publications include Tech Briefs, Technology Utilization Reports and Notes, and Technology Surveys.

Details on the availability of these publications may be obtained from:

SCIENTIFIC AND TECHNICAL INFORMATION DIVISION

NATIONAL AERONAUTICS AND SPACE ADMINISTRATION

Washington, D.C. 20546